Computers and Mathematics with Applications 80 (2020) 733–743

Contents lists available at ScienceDirect

Computers and Mathematics with Applications

journal homepage: www.elsevier.com/locate/camwa

On the spatial dynamics of vaccination: A spatial SIRS–V model

Eduardo González [a], Marcelo J. Villena [b,*]

[a] Faculty of Engineering, Universidad Finis Terrae, Chile
[b] Faculty of Engineering & Sciences, Universidad Adolfo Ibáñez, Chile

ARTICLE INFO

Article history:
Received 16 March 2016
Received in revised form 14 March 2020
Accepted 18 April 2020
Available online xxxx

Keywords:
Epidemic dynamics
Spatial SIR model
Vaccination strategy
Non-linear system of partial differential equations
Numerical modeling

ABSTRACT

In this paper, we analyze the effects of vaccination from a spatial perspective. We propose a spatial deterministic SIRS–V model, which considers a non-linear system of partial differential equations with explicit attrition and diffusion terms for the vaccination process. The model allows us to simulate numerically the spatial and temporal dynamics of an epidemic, considering different spatial strategies for the vaccination policy. In particular, in our first example we analyze the classical SIRS–V evolution with the addition of movements due to diffusion, while in the second one we focus on modeling one ring vaccination policy. We expect this model can improve spatial predictions of SIR vaccination models by taking into account the spatial dimension of the problem.

1. Introduction

Since the seminal work of Kermack and Mckendrick in 1927 [1], differential equations have been widely used to model the dynamics of infectious diseases. Currently, a large number of more sophisticated mathematical models of this family have been used to evaluate epidemics spreading, and also to formulate public health policies such as: vaccination policies, usage of face masks, quarantine, avoidance of crowded places, and so on, see for example [2–5] for reviews, and [6–8] for recent developments.

One of the main disadvantages of the SIR model is that it does not take into account the spatial dimension of the problem. Indeed, it is quite obvious that infected people have more impact on the healthy people around them. Thus, generally, for more densely populated areas it is going to take less time for a disease to spread across the region. In the same line, SIR models do not consider the possibility that populations usually relocate themselves. In this context, despite the mathematical and computational complexity of modeling epidemic dynamics in spatial settings, the potential of these tools could be very important from a policy point of view, especially considering current human mobility, see [9].

Recently, there has been growing interest in studying the spatial and temporal dynamics of infected populations, see [10–12]. In essence, classical models have been extended to reaction–diffusion equations in order to model the rate of spatial spread [4,13,14]. One of the first investigations on the spatial propagation of a disease was presented by [15]. In this paper, a reaction–diffusion equation model was developed to determine the propagation of rabies among foxes. Later, more sophisticated models were developed by Professor Murray on the same problem, see [16,17]. [10] proposed a spatial model to analyze the propagation of West Nile Virus across USA, from east to west. This model studied the propagation of the virus based on a system of partial differential reaction–diffusion equations taking the mosquito and the avian populations into account. Diffusion and advection movements were allowed for both populations, and the traveling

* Corresponding author.
E-mail addresses: e.gonzalez@ieee.org (E. González), marcelo.villena@uai.cl (M.J. Villena).

https://doi.org/10.1016/j.camwa.2020.04.015
0898-1221/

wave solutions of the model were analyzed to determine the speed of disease dissemination. From a more technical point of view, the study of traveling wave solutions of delayed reaction–diffusion equations has been a fertile avenue for the development of spatio-temporal dynamics of infected populations [12,18–22].

On the policy side, vaccination has been one of the most successful public health policies in history. Significant reductions in mortality and morbidity have been achieved via vaccination against many diseases. Furthermore, current levels of vaccination are likely to be maintained or even increased in the future [23,24]. In this context, mathematical models are key tools for evaluating alternative vaccination strategies, since they can generate predictions for comparing different strategies which can inform changes in national policy. So far, mathematical modeling has made important contributions to the understanding of the impact of vaccination programs and their designs, see for example [25–30].

Indeed, simple models can forecast vaccination coverage that will eventually help to eradicate an infectious disease. Nevertheless, in practice, the simple SIRS–V model is too naive to capture the full complexity of human populations and their interactions. For example, it is well known that human mixing is assortative, and hence the spread of infection is more likely to occur between individuals of a similar age. In this context, vaccination modeling efforts need to account for a variety of age-related effects in order to be more realistic [27,28,31]. Thus, more sophisticated and realistic analysis requires more complex modeling approaches, considering for instance, the space and time dimensions mentioned above.

Most childhood vaccines give lifelong protection, hence the policy recommendation is always to vaccinate early in life. However, when the protection offered by the vaccine is short lived, it is more efficient to target the vaccine at individuals that are most at risk. In this context, vaccination is also used to reduce the likelihood of disease outbreaks. Such reactive vaccination strategies can reduce the need of other less efficient intervention strategies. In order for vaccination policies to be effective during an outbreak, they need to be targeted in such a way that they can create a barrier between the infected individuals and the susceptible population. From a policy point of view, in this case it is clear that we need to formulate a spatial vaccination strategy in order to be more effective and efficient [28,32].

Indeed, outbreaks of a new disease tend to occur in spatial clusters, see for example [33] for foot and mouth disease epidemics, and [34] for Ebola virus outbreak in West Africa. Thus in order to model the dynamics of the disease, spatial waves of infection must be modeled, see for example [32]. In these circumstances, ring vaccination has often been shown to be an effective strategy. This strategy consists of the vaccination of all susceptible individuals in a prescribed area around an outbreak of an infectious disease. The idea is to form a buffer of immune individuals to prevent further spreading of the disease outside the vaccinated area. Ring vaccination was used to control smallpox and it has been also used successfully as a disease-control strategy, for example, to contain foot-and-mouth disease in livestock in the UK, see [35]. In this specific problem, the definition of the vaccination radius and its location are the key policy questions. Thus, in the limit, if no infected individuals escape from the ring, the infection will die out. Consequently, if the vaccination radius is too small the policy will be ineffective. On the other hand, in practical terms, to have a vaccination ring as large as possible, could be impossible from a logistic or economic point of view. Summing up, the optimal size of the vaccination ring depends upon the spatial spread of the outbreak and the speed of introduction of the vaccination campaign.

The main purpose of this paper is to study the effects of vaccination from a spatial perspective. We propose a spatial deterministic SIRS–V model, which considers a non-linear system of partial differential equations with explicit attrition and diffusion terms for the vaccination process. The model allows us to simulate numerically the spatial and temporal dynamics of an epidemic, considering different spatial strategies for the vaccination policy. In particular, in our first example we analyze the classical SIRS–V evolution with the addition of movements due to diffusion, while in the second one we focus on modeling one ring vaccination policy.

It is important to point out that without a spatial approach it is almost impossible to model the effectiveness of heterogeneous vaccination policies, a crucial matter given the scarcity of resources and the logistic restriction of universal vaccination in short periods of time. Thus, we expect this model could improve spatial predictions of SIRS–V models on vaccinations taking into account the spatial dimension of the problem. Furthermore, the possibility to simulate different spatial vaccination policies and compare the impact of each one in the territory could be a very important avenue for future research. Finally, since, this is one of the first modeling efforts in this direction, we expect this model could motivate more research in this line of work.

The rest of this paper is organized as follows. In the next section, a general formulation of the new model and its equations are presented. In Section 3, the solution of the resulting linear PDE system is numerically developed using the Crank–Nicolson Method. Two simulation examples are developed, which explore the model capabilities for studying local behavioral response to an epidemic crisis, in a spatial setting. Finally, the findings are summarized, and directions for future research are discussed.

2. Model description

In this section, we revise the basic SIRS–V model and notation. Later we introduce our basic spatial SIR model, and the modeling of responsive local movement and perception of population.

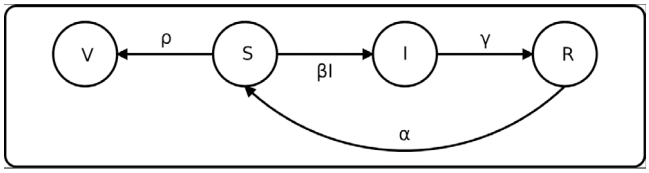

Fig. 2.1. The basic SIRS–V model.

2.1. The basic SIRS–V model

[1] in their model categorized the population as Susceptible (healthy but exposed to the disease), Infected, and Recovered. Thus, the model is usually called Susceptible–Infected–Recovered–Susceptible–Vaccinated (SIRS–V) model. We consider a basic SIRS–V model without demographics (no births, deaths and only in-bounds migration, with total population P, constant). The typical scenario here is a large naive population into which an infectious group is introduced, resulting in a fast epidemic process. This model also assumes homogeneous mixing, and that underlying epidemiological probabilities are constant. In this simple model, we also consider vaccination of susceptible individuals and assume that the vaccinated individuals are permanently immunized. Thus, we get the following SIRS–V equations:

$$\frac{\partial S}{\partial t} = -\beta SI - \rho S + \alpha R, \tag{2.1}$$

$$\frac{\partial I}{\partial t} = \beta SI - \gamma I, \tag{2.2}$$

$$\frac{\partial R}{\partial t} = \gamma I - \alpha R, \tag{2.3}$$

$$\frac{\partial V}{\partial t} = \rho S, \tag{2.4}$$

where, βSI is known as the transmission term, γ is the recovery rate, and its reciprocal represents the average infectious period. Vaccination of susceptible individuals is performed at a constant rate $\rho > 0$. α is the rate of recovered population becoming susceptible. In our model $S+I+R+V = P$, and hence with S and I, it is possible to calculate R. These equations have initial conditions $S(0) > 0$, $I(0) > 0$ and usually $R(0) = 0$ and $V(0) = 0$. The model representation is shown in 2.1, see [36] for an application of this model.

2.2. The spatial SIRS–V model

The spatial SIRS–V model uses a spatial coordinates system for the population being considered, typically four: the susceptible group, the infected group, the recovered group and the vaccinated group. Without loss of generality, the surface densities of the susceptible, infected, recovered, and vaccinated will be represented by $S(x, y, t)$, $I(x, y, t)$, $R(x, y, t)$, and $V(x, y, t)$ respectively. In the spirit of [37], each population will have an instantaneous velocity given respectively by $\vec{v}_S(x, y, t)$, $\vec{v}_I(x, y, t)$, $\vec{v}_R(x, y, t)$ and $\vec{v}_V(x, y, t)$, so the density of the flow, the amount of population per unit time that pass through a unit area, are $\vec{J}_S(x, y, t) = S(x, y, t)\,\vec{v}_S(x, y, t)$, $\vec{J}_I(x, y, t) = I(x, y, t)\,\vec{v}_I(x, y, t)$, $\vec{J}_R(x, y, t) = R(x, y, t)\,\vec{v}_R(x, y, t)$ and $\vec{J}_V(x, y, t) = V(x, y, t)\,\vec{v}_V(x, y, t)$. In addition, the net internal generation of population is defined by G_S, G_I, G_R and G_V, respectively. It should be highlighted that the surface densities S, I, R and V must be non-negatively valued functions.

Regarding the definitions presented above, the imposition of the balance of population (continuity) to the spatial dynamic of the epidemic leads to:

$$G_\theta - \vec{\nabla}\cdot\vec{J}_\theta = G_\theta - \frac{\partial J_{\theta x}}{\partial x} - \frac{\partial J_{\theta y}}{\partial y} = \frac{\partial \theta}{\partial t}\ , \tag{2.5}$$

where θ can be S, I, R or V.

It remains clear that $\vec{J}_\theta = \theta\cdot\vec{v}_\theta$, where $\vec{v}_\theta$ is the instantaneous velocity of each part of the respective moving population, and θ is the density of the respective population.

In general, the internal densities can be expressed considering the profile of the population through the SIRS–V power-series expansion:

$$G_S = g_S(x, y, t) - \sum_{i=0}^{\infty}\left\{\left(\sum_{j=0}^{\infty}\beta_{ij}S^iI^j\right) + \rho_iS^i - \alpha_iR^i\right\}\ , \tag{2.6}$$

$$G_I = g_I(x, y, t) + \sum_{i=0}^{\infty} \left\{ \left(\sum_{j=0}^{\infty} \beta_{ij} S^i I^j \right) - \gamma_i I^i \right\} . \tag{2.7}$$

$$G_R = g_R(x, y, t) + \sum_{j=0}^{\infty} \left(\gamma_i I^i - \alpha_i R^i \right) . \tag{2.8}$$

$$G_V = g_V(x, y, t) + \sum_{i=0}^{\infty} \rho_i S^i . \tag{2.9}$$

where the α_i, β_{ij}, γ_i and ρ_i coefficients are implicitly space–time dependent.

Thus, the general approach to model spatially the SIR equations can be written generically as:

$$-\vec{\nabla} \cdot (\theta \vec{v}_\theta) = \frac{\partial \theta}{\partial t} - G_\theta \tag{2.10}$$

Finally, the total number of individuals of each kind in the domain Σ, during the epidemic at any time can be found using the following expression:

$$\theta_T = \iint_{\Sigma} \theta(x, y, t) \, d\sigma \tag{2.11}$$

for example, for the susceptible population segment, we have

$$S_T(t) = \iint_{\Sigma} S(x, y, t) \, d\sigma . \tag{2.12}$$

Nevertheless, in order to complete the formulation, the motion behavior of the population must be described. In some cases explicitly through the velocities, but in other cases implicitly through the densities of the flow. The analysis performed in the next sections illustrate better this matter, specifically some particular assumptions are discussed.

2.3. Modeling responsive local movement and perception

As we discussed above, the spread of an epidemic can trigger behavioral responses of people trying to prevent themselves from catching the disease. One of the most basic preventive measures of people is to avoid infected people, either by retreating or by pushing away their health threats. We refer to this type of movement as responsive movement. Assuming that the density of the flow of populations will be related to the balance of each population, two simple possibilities should be kept in mind as main drivers of the populations (not the only ones): linear behavior of the velocities, and, linear and non-linear behavior of the densities of current.

The way a population reacts during the epidemic may vary widely depending on context and the type of population involved. Moreover, perception of the infection risk can be very different if individuals consider their own probability of infection or that of other individuals, such as family members. Lack of information means that large assumptions have to be made about people's behavior, but differing reactions in reality, both between individuals and through time, mean these assumptions may be highly unreliable; for example, reactions to an outbreak may be non-linear.

Sixteen parameters can be introduced here which account for a combined effect of the perception and risk of contagion of each population group. The first subscript indicates the observer and the second subscript indicates the subject of the observation, e.g.: h_{SI} is the result of such a combined effect of risk of contagion by the infected group, as perceived by the susceptible group. In order to separate both effects, it is useful to define the actual contagion risk of each group: k_S, k_I, k_V and k_R are assumed to be constants for this case, even though they could be time and terrain dependent, so sixteen pure parameters (u_{ij}) define just perception (in general they can be time and space dependent), and they are defined as follows:

$$\begin{bmatrix} h_{SS} & h_{SI} & h_{SR} & h_{SV} \\ h_{IS} & h_{II} & h_{IR} & h_{IV} \\ h_{RS} & h_{RI} & h_{RR} & h_{RV} \\ h_{VS} & h_{VI} & h_{VR} & h_{VV} \end{bmatrix} = \begin{bmatrix} k_S u_{SS} & k_I u_{SI} & k_R u_{SR} & k_V u_{SV} \\ k_S u_{IS} & k_I u_{II} & k_R u_{IR} & k_V u_{IV} \\ k_S u_{RS} & k_I u_{RI} & k_R u_{RR} & k_V u_{RV} \\ k_S u_{VS} & k_I u_{VI} & k_R u_{VR} & k_V u_{VV} \end{bmatrix} \tag{2.13}$$

As a rule of thumb, $h_{ij} = k_j u_{ij}$.

The group of population located at some position will move towards or away from the other population according to the perceived contagion risk of the other.

$$\vec{J}_S = -p_S \left(h_{SS} \nabla^2 S - h_{SI} \nabla^2 I - h_{SR} \nabla^2 R - h_{SV} \nabla^2 V \right) \tag{2.14}$$

$$\vec{J}_I = -p_I \left(h_{II} \nabla^2 I - h_{IS} \nabla^2 S - h_{IR} \nabla^2 R - h_{IV} \nabla^2 V \right) \tag{2.15}$$

$$\vec{J}_R = -p_R \left(h_{RR} \nabla^2 R - h_{RS} \nabla^2 S - h_{RI} \nabla^2 I - h_{RV} \nabla^2 V \right) \tag{2.16}$$

$$\vec{J}_V = -p_V \left(h_{VV}\nabla^2 R - h_{VS}\nabla^2 S - h_{VI}\nabla^2 I - h_{VV}\nabla^2 V\right) \tag{2.17}$$

where p_S, p_I, p_R and p_V are proportionality constants.

By replacing Eq. (2.15) into Eq. (2.5), and proceeding in the same way for the other forces, the densities of current no longer appear in the equations, leaving the problem with a resemblance to the classic Poisson equation in terms of the B and R force densities:

$$p_S \left(h_{SS}\nabla^2 S - h_{SI}\nabla^2 I - h_{SR}\nabla^2 R - h_{SV}\nabla^2 V\right) = \frac{\partial S}{\partial t} - G_S \tag{2.18}$$

$$p_I \left(h_{II}\nabla^2 I - h_{IS}\nabla^2 S - h_{IR}\nabla^2 R - h_{IV}\nabla^2 V\right) = \frac{\partial I}{\partial t} - G_I \tag{2.19}$$

$$p_R \left(h_{RR}\nabla^2 R - h_{RS}\nabla^2 S - h_{RI}\nabla^2 I - h_{RV}\nabla^2 V\right) = \frac{\partial R}{\partial t} - G_R \tag{2.20}$$

$$p_V \left(h_{VV}\nabla^2 R - h_{VS}\nabla^2 S - h_{VI}\nabla^2 I - h_{VV}\nabla^2 V\right) = \frac{\partial R}{\partial t} - G_R \tag{2.21}$$

Due to the generation term on the right hand side of these four equations, generally this still is a nonlinear problem. Accordingly, (2.18)–(2.21) are transformed into:

$$\begin{bmatrix} p_S h_{SS}\nabla^2 - M_S - N_S & -p_S h_{SI}\nabla^2 - E_{SI} - N_{SI} & -p_S h_{SR}\nabla^2 - E_{SR} - N_{SR} & -p_S h_{SV}\nabla^2 - E_{SV} - N_{SV} \\ -p_I h_{IS}\nabla^2 - E_{IS} - N_{IS} & p_I h_{II}\nabla^2 - M_I - N_I & -p_I h_{IR}\nabla^2 - E_{IR} - N_{IR} & -p_I h_{IV}\nabla^2 - E_{IR} - N_{IV} \\ -p_R h_{RS}\nabla^2 - E_{RS} - N_{RS} & -p_R h_{RI}\nabla^2 - E_{RI} - N_{RI} & p_R h_{RR}\nabla^2 - M_R - N_R & p_R h_{RV}\nabla^2 - E_{RV} - N_{RV} \\ -p_V h_{VS}\nabla^2 - E_{VS} - N_{VS} & -p_V h_{VI}\nabla^2 - E_{VI} - N_{VI} & p_V h_{VR}\nabla^2 - E_{VR} - N_{VR} & p_V h_{VV}\nabla^2 - M_V - N_V \end{bmatrix} \begin{bmatrix} S \\ I \\ R \\ V \end{bmatrix} = \frac{\partial}{\partial t}\begin{bmatrix} S \\ I \\ R \\ V \end{bmatrix} \tag{2.22}$$

where a new subscript has been added to the E coefficients, because they represent links between more than just one population. Now defining:

$$[\mathcal{L}] = \overbrace{\begin{bmatrix} p_S h_{SS} & -p_S h_{SI} & -p_S h_{SR} & -p_S h_{SV} \\ -p_I h_{IS} & p_I h_{II} & -p_I h_{IR} & -p_I h_{IV} \\ -p_R h_{RS} & -p_R h_{RI} & p_R h_{RR} & p_R h_{RV} \\ -p_V h_{VS} & -p_V h_{VI} & p_V h_{VR} & p_V h_{VR} \end{bmatrix}}^{[Q]} \nabla^2 - \overbrace{\overbrace{\begin{bmatrix} W_1 & E_{SI} & E_{SR} & E_{SV} \\ E_{IS} & W_2 & E_{IR} & E_{IV} \\ E_{RS} & E_{RI} & W_3 & E_{RV} \\ E_{VS} & E_{VI} & E_{VR} & W_4 \end{bmatrix}}^{E} + \overbrace{\begin{bmatrix} N_S & N_{SI} & N_{SR} & N_{SV} \\ N_{IS} & N_I & N_{IR} & N_{IV} \\ N_{RS} & N_{RI} & N_R & N_{RV} \\ N_{VS} & N_{VI} & N_{VR} & N_V \end{bmatrix}}^{\Phi}}^{[W]} \tag{2.23}$$

where Φ represents a nonlinear operator.

3. Numerical solution for a 2D grid

As S, I, R and V must be non negatively valued at each point of the space–time domain, the solution to this problem cannot be treated as in the Dirichlet or Neumann formulation, because the non negativity can be regarded as a time dependent border condition. Bearing in mind this statement, a numerical approach suits this problem better, where the formulation given by Eq. (2.22) drives to a time stepping formulation for the spatial profile of the S, I, R and V scalar fields. The procedure should provide a way to adjust the time step so as to limit the maximum deviation of negative values and then to reset acceptable deviations to zero. The time stepping can be faced with a Crank–Nicolson (C–N) method, leaving the spatial problem to other methods. Here, Finite Differences (FD) are used as a first approach.

As we saw early, Eq. (2.22) can be rewritten as:

$$[\mathcal{L}] = [Q]\nabla^2 - [W] - [\Phi] \tag{3.1}$$

$$F(U) \doteq \left\{[Q]\nabla^2 - [W] - [\Phi]\right\}[U] = [I]\frac{\partial}{\partial t}[U] \tag{3.2}$$

Crank–Nicolson decomposition leads to:

$$\frac{1}{2}\left(\left[F\left(\left[U^{n+1}\right]\right)\right] + \left[F\left(\left[U^{n}\right]\right)\right]\right) = \frac{1}{\Delta t}[I]\left(\left[U^{n+1}\right] - \left[U^{n}\right]\right), \tag{3.3}$$

or,

$$-[Q]\nabla^2\left[U^{n+1}\right]+\left(\frac{2}{\Delta t}[I]+[W]\right)\left[U^{n+1}\right]=[Q]\nabla^2\left[U^{n}\right]+\left(\frac{2}{\Delta t}[I]-[W]\right)\left[U^{n}\right] \tag{3.4}$$

and application of FD for square elements ($\Delta x=\Delta y$) for the Laplacian Operator yields:

$$\nabla^2 F\sim\frac{1}{(\Delta x)^2}\left(F_{i-1,j}+F_{i,j-1}+F_{i,j+1}+F_{i+1,j}-4F_{i,j}\right) \tag{3.5}$$

which allows us to write:

$$\begin{aligned}&-\frac{1}{(\Delta x)^2}[Q]\left(\left[U^{n+1}_{i-1,j}\right]+\left[U^{n+1}_{i,j-1}\right]+\left[U^{n+1}_{i,j+1}\right]+\left[U^{n+1}_{i+1,j}\right]-4\left[U^{n+1}_{i,j}\right]\right)+\left(\frac{2}{\Delta t}[I]+[W]\right)\left[U^{n+1}_{i,j}\right]=\\&\frac{1}{(\Delta x)^2}[Q]\left(\left[U^{n}_{i-1,j}\right]+\left[U^{n}_{i,j-1}\right]+\left[U^{n}_{i,j+1}\right]+\left[U^{n}_{i+1,j}\right]-4\left[U^{n}_{i,j}\right]\right)+\left(\frac{2}{\Delta t}[I]-[W]\right)\left[U^{n}_{i,j}\right]\end{aligned} \tag{3.6}$$

Now, by assuming that the grid to be considered has L by M square cells of side Δx, that $[U]$ represents a vector which holds S, I, R and V populations, that $[I_{LM}]$ the identity matrix of $LM\times LM$ dimension, and that $[I_{2LM}]$ is the identity matrix of $2LM\times 2LM$ dimension, then the equation turns into:

$$\left\{\frac{2}{\Delta t}\left[I_{2LM}\right]+\begin{bmatrix}\left(W_1+N_S\right)\left[I_{LM}\right]+[Z_1]-\frac{Q_{SS}}{(\Delta x)^2}[S] & \left(E_{SI}+N_{SI}\right)\left[I_{LM}\right]-\frac{Q_{SI}}{(\Delta x)^2}[S] & \left(E_{SR}+N_{SR}\right)\left[I_{LM}\right]-\frac{Q_{SR}}{(\Delta x)^2}[S] & \left(E_{SV}+N_{SV}\right)\left[I_{LM}\right]-\frac{Q_{SV}}{(\Delta x)^2}[S]\\ \left(E_{IS}+N_{IS}\right)\left[I+Z_{LM}\right]-\frac{Q_{IS}}{(\Delta x)^2}[S] & \left(W_2+N_I\right)\left[I_{LM}\right]+[Z_2]-\frac{Q_{II}}{(\Delta x)^2}[S] & \left(E_{IR}+N_{IR}\right)\left[I_{LM}\right]-\frac{Q_{IR}}{(\Delta x)^2}[S] & \left(E_{IV}+N_{IV}\right)\left[I_{LM}\right]-\frac{Q_{IV}}{(\Delta x)^2}[S]\\ \left(E_{RS}+N_{RS}\right)\left[I_{LM}\right]-\frac{Q_{RS}}{(\Delta x)^2}[S] & \left(E_{RI}+N_{RI}\right)\left[I_{LM}\right]-\frac{Q_{RI}}{(\Delta x)^2}[S] & \left(W_3+N_R\right)\left[I_{LM}\right]+[Z_3]-\frac{Q_{RR}}{(\Delta x)^2}[S] & \left(E_{RV}+N_{RV}\right)\left[I_{LM}\right]-\frac{Q_{RV}}{(\Delta x)^2}[S]\\ \left(E_{VS}+N_{VS}\right)\left[I_{LM}\right]-\frac{Q_{VS}}{(\Delta x)^2}[S] & \left(E_{VI}+N_{VI}\right)\left[I_{LM}\right]-\frac{Q_{VI}}{(\Delta x)^2}[S] & \left(E_{VR}+N_{VR}\right)\left[I_{LM}\right]-\frac{Q_{VR}}{(\Delta x)^2}[S] & \left(W_4+N_V\right)\left[I_{LM}\right]+[Z_4]-\frac{Q_{VV}}{(\Delta x)^2}[S]\end{bmatrix}\right\}\left[U^{n+1}\right]=$$

$$\left\{\frac{2}{\Delta t}\left[I_{2LM}\right]-\begin{bmatrix}\left(W_1+N_S\right)\left[I_{LM}\right]+[Z_1]-\frac{Q_{SS}}{(\Delta x)^2}[S] & \left(E_{SI}+N_{SI}\right)\left[I_{LM}\right]-\frac{Q_{SI}}{(\Delta x)^2}[S] & \left(E_{SR}+N_{SR}\right)\left[I_{LM}\right]-\frac{Q_{SR}}{(\Delta x)^2}[S] & \left(E_{SV}+N_{SV}\right)\left[I_{LM}\right]-\frac{Q_{SV}}{(\Delta x)^2}[S]\\ \left(E_{IS}+N_{IS}\right)\left[I_{LM}\right]-\frac{Q_{IS}}{(\Delta x)^2}[S] & \left(W_2+N_I\right)\left[I_{LM}\right]+[Z_2]\frac{Q_{II}}{(\Delta x)^2}[S] & \left(E_{IR}+N_{IR}\right)\left[I_{LM}\right]-\frac{Q_{IR}}{(\Delta x)^2}[S] & \left(E_{IV}+N_{IV}\right)\left[I_{LM}\right]-\frac{Q_{IV}}{(\Delta x)^2}[S]\\ \left(E_{RS}+N_{RS}\right)\left[I_{LM}\right]-\frac{Q_{RS}}{(\Delta x)^2}[S] & \left(E_{RI}+N_{RI}\right)\left[I_{LM}\right]-\frac{Q_{RI}}{(\Delta x)^2}[S] & \left(W_3+N_R\right)\left[I_{LM}\right]+[Z_3]-\frac{Q_{RR}}{(\Delta x)^2}[S] & \left(E_{RV}+N_{RV}\right)\left[I_{LM}\right]-\frac{Q_{RV}}{(\Delta x)^2}[S]\\ \left(E_{VS}+N_{VS}\right)\left[I_{LM}\right]-\frac{Q_{VS}}{(\Delta x)^2}[S] & \left(E_{VI}+N_{VI}\right)\left[I_{LM}\right]-\frac{Q_{VI}}{(\Delta x)^2}[S] & \left(E_{VR}+N_{VR}\right)\left[I_{LM}\right]-\frac{Q_{VR}}{(\Delta x)^2}[S] & \left(W_4+N_V\right)\left[I_{LM}\right]+[Z_4]-\frac{Q_{VV}}{(\Delta x)^2}[S]\end{bmatrix}_{(1)}\right\}\left[U^{n}\right] \tag{3.7}$$

where $[S]$ is the matrix generated from the assembly given by the Laplacian operator,

$$[Z_1]=v_{0Sx}[X]+v_{0Sy}[Y] \tag{3.8}$$

$$[Z_2]=v_{0Ix}[X]+v_{0Iy}[Y] \tag{3.9}$$

$$[Z_3]=v_{0Rx}[X]+v_{0Ry}[Y] \tag{3.10}$$

$$[Z_4]=v_{0Vx}[X]+v_{0Vy}[Y] \tag{3.11}$$

where $[X]$ and $[Y]$ are generated by using respectively the differential operators given by:

$$\frac{\partial H}{\partial x}\sim\frac{1}{2(\Delta x)}\left(H_{i+1,j}-H_{i-1,j}\right) \tag{3.12}$$

$$\frac{\partial H}{\partial y}\sim\frac{1}{2(\Delta x)}\left(H_{i,j+1}-H_{i,j-1}\right) \tag{3.13}$$

Clearly, Eq. (3.7) gives a procedure to solve $[U]$ by stepping, but in order to include a convergent solution for this nonlinear problem, we also include a variable number of iterations at each step. Eq. (3.7) presents separately the time and spatial evolution of the populations. Indeed, if $[Q_i=0]$, then the system becomes the traditional SIR model, without a spatial component.

As expected, all the terms in the matrices are constant and hopefully positive. If a negative but tolerable value, i.e. a small enough value, appears in one of the components of the vector $\begin{pmatrix}S\\I\\R\\V\end{pmatrix}$ then that negative term must be replaced by a zero because only positive populations are significant here. If for some element of that vector the negative value is too large, then it is advisable to repeat the procedure for the last step with a smaller value of Δt.

4. Simulation examples

Our first example takes the following values for the attrition or conversion processes:

$$[E]=\begin{bmatrix}-0.002 & 0.0 & 0.02 & 0.0\\ 0.0 & -0.3 & 0.0 & 0.0\\ 0.0 & 0.3 & -0.02 & 0.0\\ 0.002 & 0.0 & 0.0 & 0.0\end{bmatrix},\qquad [\Phi(S,I)]=\begin{bmatrix}-29.7\cdot I & 0.0 & 0.0 & 0.0\\ 0.0 & 29.7\cdot S & 0.0 & 0.0\\ 0.0 & 0.0 & 0.0 & 0.0\\ 0.0 & 0.0 & 0.0 & 0.0\end{bmatrix}$$

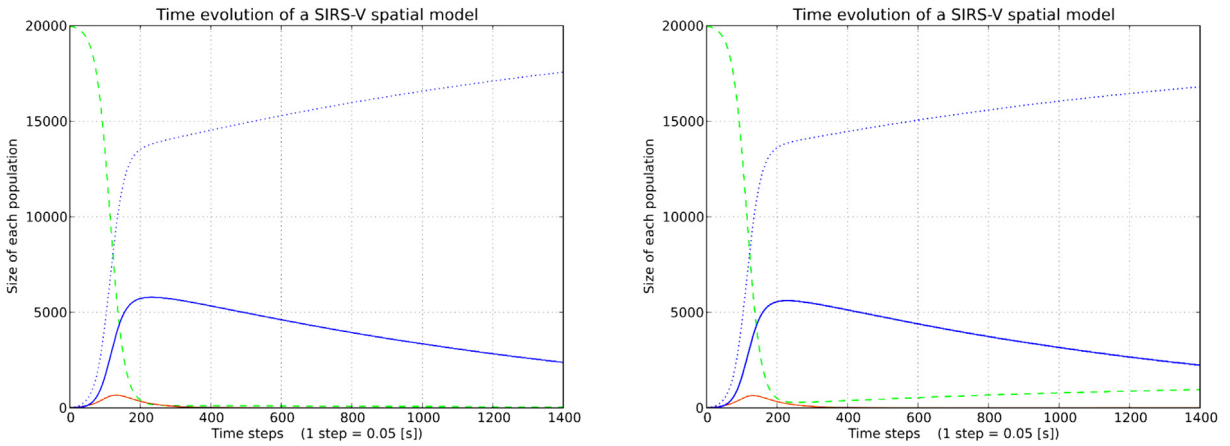

Fig. 4.1. Time evolution of a SIRS–V spatial model, (1:left) low diffusion, and (2:right) high diffusion. Dashed Green (S), Solid Red(I), Solid Blue(R) and Dotted Blue (V).

The perception parameters are all nil except $h_{IS} = 0.1$, $h_{II} = 1.0$, $h_{RI} = -1.0$ and $h_{RR} = -0.2$ so the infected population will move away from the susceptible population each time they have less local concentration of population from the latter. On the other hand, the recovered population will nearly always move away from the infected ones.

We analyze two cases of proportionality constants, $p_i^{(1)} = 0.01$ and $p_i^{(2)} = 11.5$. $(i = S, I, R, V)$. We use 1400 time-steps for a time-horizon of 70 s, on a grid of $37 \times 25 = 925$ nodes. The evolution of the total populations is rather similar except for the fact that the susceptible population will start to grow after reaching a minimum. Other changes are also visible when comparing both plots (see Fig. 4.1).

An explanation for the different behavior lies in the fact that diffusion makes part of the recovered population to return near the susceptible population, thus increasing the local concentration of those forces, then increasing the size of susceptible population whilst the infected population is no longer there, but in an outer ring surrounding the susceptible population. Fine details can be seen for the low diffusion case (2) in Fig. 4.2, whilst the high diffusion case is shown as case (3) in Fig. 4.2. The difference is very clear between these two cases, and we see that the recovered population tends to quickly move away from the infected population; the rationale for this imposed behavior is that the recovered population will eventually turn into susceptible subjects exposed to contagion (if locally they have infected neighbors).

It is important to notice that the first plot in Fig. 4.2 predicts a negligible size of infected population, from time-step 300, while the second plot forecasts a growing size of the infected population. A non-spatial model would not be able to predict these differences.

The second example considers a population spread over a domain, where the health authority has spotted a circular area of radius equal to 169 m that appears to contain an infected population. The health authority does not have accurate knowledge on the real placement of the outbreaks of the epidemic or how many individual outbreaks there are. In reality there are three outbreaks, centered at (−75 m, 75 m), (75 m, 75 m) and (−75 m, −75 m) respectively, with two having a radius of 30 m, and the third 25 m. The origin of the coordinates is at the center of the domain.

In this context, the vaccination process occurs inside a circle of a radius of 169 m where the previously described outbreaks are embedded. The vaccination is only for the susceptible population, so the infected and the recovered are not vaccinated. Recovered persons do not spread until they are again susceptible.

The populations behave exactly as in the first example ($h_{IS} = 0.1$, $h_{II} = 1.0$, $h_{RI} = -1.0$ and $h_{RR} = -0.2$), but with the following matrices:

$$[E] = 10^{-6}\begin{bmatrix} -2.0 & 0.0 & 20.0 & 0.0 \\ 0.0 & -300.0 & 0.0 & 0.0 \\ 0.0 & 300.0 & -20.0 & 0.0 \\ 2.0 & 0.0 & 0.0 & 0.0 \end{bmatrix}, \qquad [\Phi\,(S, I)] = 10^{-6}\begin{bmatrix} -29.7 \cdot I & 0.0 & 0.0 & 0.0 \\ 0.0 & 29.7 \cdot S & 0.0 & 0.0 \\ 0.0 & 0.0 & 0.0 & 0.0 \\ 0.0 & 0.0 & 0.0 & 0.0 \end{bmatrix}$$

The proportionality constants are defined by $p_i = 0.0115$ for $(i = S, I, R, V)$. We consider the time evolution for 40 days by using 1400 time-steps on a spatial grid of $47 \times 47 = 2209$ nodes. Recovered persons not spread until they are again susceptible.

The time evolution of individuals after the start of the epidemic with ring vaccination is shown in Fig. 4.3. At first sight, looking the time evolution, it seems that the campaign succeeds but looking carefully, and given the bounds for the vaccination program, it is clear that the infection will keep growing outside that region, thus the infection is defeated inside the vaccination circle but not eradicated: actually with an initial outbreak of 1000 over a total population of 20 thousand, the model forecasts that at the second day the infected group would reduce to only 17 individuals, hinting an

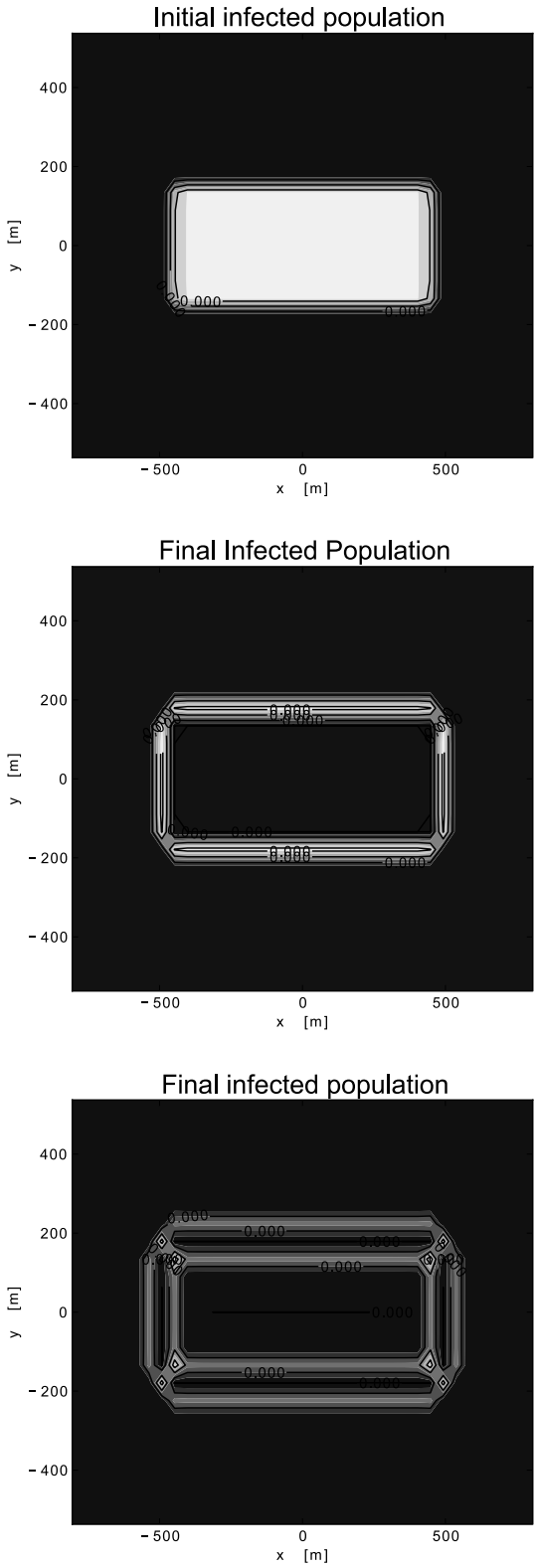

Fig. 4.2. Snapshots of the distribution of the infected population concentrations for low and high diffusion 1: Baseline case, 2: Low diffusion case, 3: High diffusion case. (Lighter shade implies higher concentration).

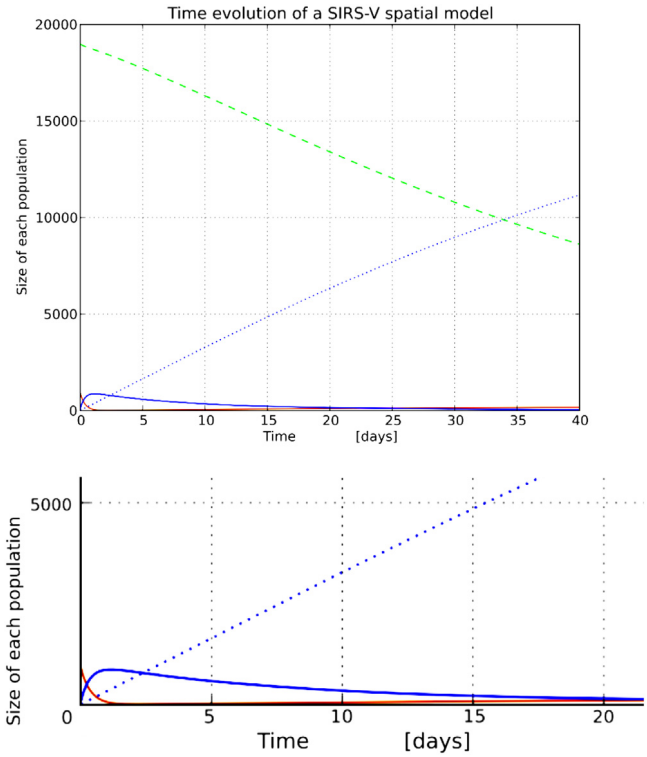

Fig. 4.3. Snapshots of the distribution of the population concentrations with a restricted area of vaccination. Dashed Green (S), Solid Red(I), Solid Blue(R) and Dotted Blue (V). Each step is 246 [s]. A zoom of the left corner of the first figure is presented in the figure below it.

erroneous success, because from that day the infected group will grow quite steadily reaching the figure of 173 by day 40.

The spatial distributions of infected at three points over the 40-day simulation are shown in Fig. 4.4. In the contour plot, lighter shades mean higher concentrations, show that the rejection of the susceptible group makes the speed of diffusion of the infected subjects high enough to escape off the vaccination circle. Regarding this, it could have been wiser to increase the vaccination rate near the circle border or to increase the radius of the vaccination circle. Notice that one part of the small group of infected population managed to stay in the circle, perhaps due to the displacement of the susceptible population to safer places between the pocket of infected population and the outer ring of the unhealthy group. The other groups of infected population have disappeared from within the circle, mainly because their introspective attitude depended on their higher concentration which reduced their escaping attitude, making them more exposed to vaccination, while keeping the susceptible population less keen on running away.

5. Conclusions

The spatial considerations in the definition of vaccination policies have proven to be vital to eradicate several epidemics. Despite of this, there are scarce research efforts in this direction. In this paper, we present a first model that allows us to model different spatial vaccination policies such as the ring vaccination policy. In particular, we propose a spatial deterministic SIRS–V model, formed by a non-linear system of partial differential equations with explicit attrition and diffusion terms for the vaccination process. The model is very flexible to simulate different locations and population densities and their diffusion, and hence to measure the effectiveness of spatial vaccination policies, a crucial and contemporary matter given the scarcity of resources and the velocity required for health authorities to eradicate epidemics with fast spreading.

Our first example forecasts deviations when using different diffusion values (i.e. comparing what happens with the recovered population at 400 time-steps, the vaccinated population at 600 hundred time-steps and the infected population after 400 time-steps), as the diffusive model is more realistic than the traditional time-dependent models for this simple stance, with more complex boundary conditions, the differences should be even more relevant.

In our second example, we see that a larger local imbalance of infected population can result in quick runaways to places where vaccination is not covered, resulting in a new source for spreading the disease, thus causing more toil and eventually increasing costs. This model, applied to vaccination campaigns can be used to simulate different vaccination

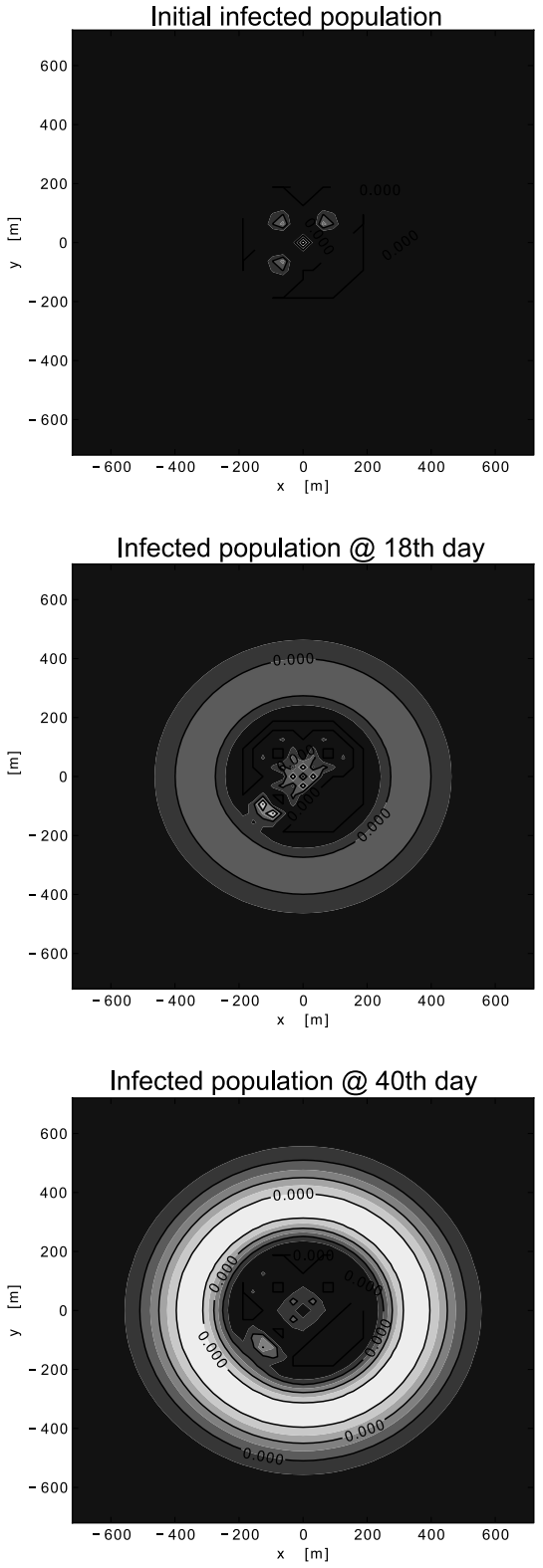

Fig. 4.4. Snapshots of the distribution of the infected population concentrations with a restricted area of vaccination. (Lighter shade implies higher concentration.)

coverages in order to succeed in reducing the population-time infection. It must be stressed that the traditional purely time-dependent model is not useful for dealing with these space–time evolution of SIRS–V problems.

In the near future, we expect to refine the model by considering more complex attitude descriptions including remote effects while, in terms of attrition, the model requires to include non-linear terms for the exchange rates. Other enhancements to this model should consider death rates, specially for long term or chronic diseases, and could include age segmentation for each of the groups. As the model is expanded, more resources will be needed, including parallel processing to obtain results in reasonable times. An even better model would make the circle a remote attractor for the susceptible population outside the circle.

The results shown here encourage further research in order to decide on the best strategy to efficiently cope with an epidemic outbreak. With proper care of the stabilization problems, this spatial modeling of epidemics can be useful for cases where birth/death take place or when mobile infected population can create a variable outbreak of a disease.

CRediT authorship contribution statement

Eduardo González: Conceptualization, Methodology, Software, Writing - original draft, Writing - review & editing. **Marcelo J. Villena:** Conceptualization, Methodology, Software, Writing - original draft, Writing - review & editing.

Acknowledgment

Aid from the Fondecyt Program, Chile, project Nº 1131096, is gratefully acknowledged by the authors.

References

[1] W.O. Kermack, A.G. McKendrick, A contribution to the mathematical theory of epidemics, in: Proceedings of the Royal Society of London A: Mathematical, Physical and Engineering Sciences, Vol. 115, The Royal Society, 1927, pp. 700–721, no. 772.
[2] A. Okubo, Diffusion and Ecological Problems; Mathematical Models, Tech. Rep., 1980.
[3] R.M. Anderson, R.M. May, B. Anderson, Infectious Diseases of Humans: Dynamics and Control, Vol. 28, Wiley Online Library, 1992.
[4] J. Heesterbeek, Mathematical Epidemiology of Infectious Diseases: Model Building, Analysis and Interpretation, Vol. 5, John Wiley & Sons, 2000.
[5] F. Brauer, C. Castillo-Chavez, C. Castillo-Chavez, Mathematical Models in Population Biology and Epidemiology, Vol. 40, Springer, 2001.
[6] A. Ibeas, M. de la Sen, S. Alonso-Quesada, Robust sliding control of SEIR epidemic models, Math. Probl. Eng. 2014 (2014).
[7] J. Hui, J.-H. Pang, D.-R. Lin, Mathematical analysis of an epidemic-species hybrid dynamical system, Math. Probl. Eng. 2014 (2014).
[8] Z. Liu, C.-T. Fang, A modeling study of human infections with avian influenza A H7N9 virus in mainland China, Int. J. Infec. Dis. 41 (2015) 73–78.
[9] D. Brockmann, V. David, A.M. Gallardo, Human mobility and spatial disease dynamics, Rev. Nonlinear Dyn. Complex. 2 (2009) 1–24.
[10] N.A. Maidana, H.M. Yang, Spatial spreading of West Nile Virus described by traveling waves, J. Theoret. Biol. 258 (3) (2009) 403–417.
[11] G.-Q. Sun, Pattern formation of an epidemic model with diffusion, Nonlinear Dynam. 69 (3) (2012) 1097–1104.
[12] Z. Wang, R. Xu, Travelling waves of a diffusive epidemic model with latency and relapse, Discrete Dyn. Nat. Soc. 2013 (2013).
[13] J. Murray, Mathematical Biology: Spatial Models and Biomedical Applications, Volume II, Springer-Verlag, Berlin Heidelberg, Germany, 2003.
[14] R.S. Cantrell, C. Cosner, Spatial Ecology via Reaction-Diffusion Equations, John Wiley & Sons, 2004.
[15] A. Källen, P. Arcuri, J. Murray, A simple model for the spatial spread and control of rabies, J. Theoret. Biol. 116 (3) (1985) 377–393.
[16] J. Murray, E. Stanley, D. Brown, On the spatial spread of rabies among foxes, Proc. R. Soc. Lond. Ser. B: Biol. Sci. 229 (1255) (1986) 111–150.
[17] J. Murray, W. Seward, On the spatial spread of rabies among foxes with immunity, J. Theoret. Biol. 156 (3) (1992) 327–348.
[18] J. Al-Omari, S.A.s. Gourley, Stability and traveling fronts in Lotka-Volterra competition models with stage structure, SIAM J. Appl. Math. 63 (6) (2003) 2063–2086.
[19] Q. Gan, R. Xu, X. Zhang, P. Yang, Travelling waves of a three-species Lotka–Volterra food-chain model with spatial diffusion and time delays, Nonlinear Anal. RWA 11 (4) (2010) 2817–2832.
[20] Q.-R. Wang, K. Zhou, Traveling wave solutions in delayed reaction–diffusion systems with mixed monotonicity, J. Comput. Appl. Math. 233 (10) (2010) 2549–2562.
[21] S. Chinviriyasit, W. Chinviriyasit, Numerical modelling of an SIR epidemic model with diffusion, Appl. Math. Comput. 216 (2) (2010) 395–409.
[22] S. Zhang, R. Xu, Travelling waves and global attractivity of an SIRS disease model with spatial diffusion and temporary immunity, Appl. Math. Comput. 224 (2013) 635–651.
[23] M. Keeling, M. Tildesley, T. House, L. Danon, The mathematics of vaccination, Math. Today 49 (2013) 40–43.
[24] J.N. Hays, Epidemics and Pandemics: Their Impacts on Human History, Abc-clio, 2005.
[25] M. Alexander, C. Bowman, S. Moghadas, R. Summers, A. Gumel, B. Sahai, A vaccination model for transmission dynamics of influenza, SIAM J. Appl. Dyn. Syst. 3 (4) (2004) 503–524.
[26] B. Cantó, C. Coll, E. Sánchez, A study on vaccination models for a seasonal epidemic process, Appl. Math. Comput. 243 (2014) 152–160.
[27] Z. Feng, S. Towers, Y. Yang, Modeling the effects of vaccination and treatment on pandemic influenza, AAPS J. 13 (3) (2011) 427–437.
[28] C.J.E. Metcalf, V. Andreasen, O.N. Bjørnstad, K. Eames, W.J. Edmunds, S. Funk, T.D. Hollingsworth, J. Lessler, C. Viboud, B.T. Grenfell, Seven challenges in modeling vaccine preventable diseases, Epidemics 10 (2015) 11–15.
[29] S. Moghadas, Modelling the effect of imperfect vaccines on disease epidemiology, Discrete Contin. Dyn. Syst. Ser. B 4 (2004) 999–1012.
[30] A. Scherer, A. McLean, Mathematical models of vaccination, British Med. Bull. 62 (1) (2002) 187–199.
[31] J. Glasser, D. Taneri, Z. Feng, J.-H. Chuang, P. Tüll, W. Thompson, M.M. McCauley, J. Alexander, Evaluation of targeted influenza vaccination strategies via population modeling, PLoS One 5 (9) (2010) e12777.
[32] S. Riley, Large-scale spatial-transmission models of infectious disease, Science 316 (5829) (2007) 1298–1301.
[33] M.J. Keeling, M.E. Woolhouse, D.J. Shaw, L. Matthews, M. Chase-Topping, D.T. Haydon, S.J. Cornell, J. Kappey, J. Wilesmith, B.T. Grenfell, Dynamics of the 2001 UK foot and mouth epidemic: stochastic dispersal in a heterogeneous landscape, Science 294 (5543) (2001) 813–817.
[34] M.W. Carroll, D.A. Matthews, J.A. Hiscox, M.J. Elmore, G. Pollakis, A. Rambaut, R. Hewson, I. García-Dorival, J.A. Bore, R. Koundouno, et al., Temporal and spatial analysis of the 2014-2015 Ebola virus outbreak in West Africa, Nature (2015).
[35] M. Keeling, M. Woolhouse, R. May, G. Davies, B. Grenfell, Modelling vaccination strategies against foot-and-mouth disease, Nature 421 (6919) (2003) 136–142.
[36] L. Misici, F. Santarelli, Epidemic propagation: An automaton model as the continuous SIR model, Appl. Math. 4 (10) (2013) 84.
[37] E. González, M. Villena, Spatial lanchester models, European J. Oper. Res. 210 (3) (2011) 706–715.